Giant neutron halos in the non-relativistic mean field approach

M. Grasso,[1,2,3] S. Yoshida,[1,4] N. Sandulescu,[5,6] and N. Van Giai[1]
[1]*Institut de Physique Nucléaire, 15 rue Georges Clémenceau, F-91406 Orsay Cedex, France*
[2]*Dipartimento di Fisica e Astronomia, Via Santa Sofia 64, I-95123 Catania, Italy*
[3]*INFN, Sezione di Catania, Via Santa Sofia 64, I-95123 Catania, Italy*
[4]*Science Research Center, Hosei University, 2-17-1 Fujimi, Chiyoda, Tokyo 102-8160, Japan*
[5]*Service de Physique Nucléaire, CEA-DAM Ile-de-France, BP 12, F-91680 Bruyères-le-Châtel, France*
[6]*Institute for Physics and Nuclear Engineering, P.O. Box MG-6, RO-76900 Bucharest, Romania*
(Received 23 March 2006; published 26 December 2006)

Giant neutron halos in medium-heavy nuclei are studied in the framework of the Hartree-Fock-Bogoliubov (HFB) approach with Skyrme interactions. The appearance of such structures depends sensitively on the effective interaction adopted. This is illustrated by comparing the predictions of SLy4 and SkI4 in the Ca and Zr isotopic chains. The latter force predicts a neutron halo in the Zr chain with $A > 122$ due to the weakly bound orbitals $3p1/2$ and $3p3/2$. It is found that the energies of states near the separation threshold depend sensitively on effective mass values. The structure of the halo is analyzed in terms of the occupation probabilities of these orbitals and their partial contributions to the neutron density. The antihalo effect is also discussed in the case of ^{124}Zr by comparing the occupation probabilities and wave functions of the Hartree-Fock neutron single-particle states near the Fermi energy with the corresponding HFB quasiparticle states.

DOI: 10.1103/PhysRevC.74.064317 PACS number(s): 21.10.Gv, 21.10.Pc, 21.60.Jz, 27.40.+z

I. INTRODUCTION

Currently, several projects for the construction of a new generation of radioactive beam facilities are in progress (see, e.g., Ref. [1]). Such facilities will permit researchers to investigate the properties of unstable nuclei situated close to drip-line regions. From the theoretical side, many efforts are devoted to performing accurate predictions to locate the proton and neutron drip lines as well as to describe the behavior of unstable nuclei. Unfortunately, theoretical predictions in exotic regions of the nuclear chart can be rather model dependent.

Self-consistent mean field methods are well-suited theoretical tools for describing medium and heavy nuclei. There are two main lines of investigation based on the mean field approach, namely, the relativistic mean field (RMF) method, which treats effective Lagrangians in the Hartree approximation, and the nonrelativistic Hartree-Fock (HF) method, which uses effective interactions such as the Gogny and Skyrme forces. Recent reviews can be found in Refs. [2,3]. When approaching the drip lines, one deals with open-shell nuclei for which the effects of pairing correlations become quite important, especially for such properties as the tails of matter distributions. The pairing correlations can be described by the nonrelativistic Hartree-Fock-Bogoliubov (HFB) theory [4,5] or by the relativistic Hartree-Bogoliubov (RHB) theory. The most widely used choice is to add a phenomenological pairing interaction acting in the particle-particle channel [6]. Alternatively, one can use the same meson-nucleon Lagrangian to generate the particle-particle interaction, then make a zero-range approximation, and finally readjust the particle-particle interaction by an overall factor [7].

Furthermore, the chemical potential λ becomes close to zero in the vicinity of drip lines, and it is necessary to treat properly the contributions of the quasiparticle continuum when evaluating the pairing correlations [5]. Thus, the most appropriate approach for such cases is to solve the self-consistent mean field equations in coordinate space, and this is the method we use to obtain the results of this work.

A very interesting phenomenon has been recently predicted within the RHB approach: the formation of a neutron giant halo (with up to six neutrons involved) in some very neutron-rich isotopes. The radius of the neutron distribution as a function of A shows a kink at the nucleus where the halo structure starts to be formed. This effect has been found to be particularly strong in Ca (with $A > 60$) [8] and Zr (with $A > 122$) [9] isotopes. These predictions are based on the NLSH parametrization, and similar results are obtained with the TM1 parametrization [10]. The giant halo phenomenon is also found in the near-drip-line Zr isotopes if one uses the NL3 parametrization in an RMF plus resonant continuum BCS [11]. The giant halo effect in medium-heavy nuclei has been much less investigated within the nonrelativistic mean field approach, apart from Ref. [12], where the halo phenomenon is studied in Ni and Sn, and Ref. [13] for Ca isotopes. The purpose of the present work is to investigate the giant halo effect in Ca and Zr isotopes within the nonrelativistic Skyrme-Hartree-Fock-Bogoliubov mean field approach. This effect may appear in the vicinity of drip lines, if at all, and therefore it is probably still out of reach of the next generation facilities.

Important discrepancies are often found in the position of the neutron drip line predicted by different models. For instance, these differences clearly appear in the neutron drip line of Ni isotopes calculated in relativistic [14] and nonrelativistic [5] approaches. Even among parametrizations of the Skyrme force used in HFB calculations, one can obtain different drip-line predictions. It is found in Ref. [13] that drip lines in Ca isotopes occur for heavier systems if one uses SkM* rather than the widely used SLy4. In this work, we find that the parametrization SkI4 [15] also leads to bound Ca and

Zr isotopes with a larger neutron excess than SLy4. Thus, it is foreseen that giant halo predictions based on the Skyrme-HFB approach will suffer from some model dependences. While waiting for new experimental data that will help discriminate among the available models, it would be interesting to analyze the reasons for some of these discrepancies.

For our analysis, we choose two Skyrme parametrizations, namely, SLy4, which is commonly adopted to treat neutron-rich systems since it includes constraints coming from the neutron matter equation of state, and the SkI4 energy functional of Reinhard and Flocard [15]. The reason for the latter choice is simply that it leads to bound Zr isotopes having more neutrons than the SLy4 force, and, hence, the giant halo phenomenon can take place. As for the Ca isotopes, neither SLy4 nor SkI4 can produce bound Ca isotopes that are neutron rich enough to lead to a halo effect.

The present calculations include pairing correlation effects, and these correlations can induce an antihalo effect, as pointed out in Ref. [16]. We discuss this effect in the case of the ^{124}Zr nucleus by comparing the HFB results with the corresponding HF ones.

The article is organized as follows. In Sec. II, we briefly describe the theoretical framework. In Sec. III A, we present the two-neutron separation energies, neutron radii, and HF single-particle spectra for neutron-rich Ca and Zr isotopes, and we compare our nonrelativistic results with the corresponding RHB results obtained with the NLSH parametrization [8,9]. We discuss the differences found in the HF spectra with the adopted Skyrme parametrizations by analyzing, in some cases, the mean field and spin-orbit contributions to the total potential. In Sec. III B, we consider in more detail the case of Zr isotopes and investigate giant halo and antihalo effects by analyzing occupation probabilities, neutron density profiles, and wave function tails. In Sec. IV, our conclusions are drawn.

II. THEORETICAL FRAMEWORK

The theoretical framework used in this paper is the HFB approach. For zero-range two-body forces, the HFB equations have the form

$$\begin{aligned}[h(\mathbf{r}) - \lambda]u(E,\mathbf{r}) + \Delta(\mathbf{r})v(E,\mathbf{r}) &= Eu(E,\mathbf{r}),\\ \Delta(\mathbf{r})u(E,\mathbf{r}) - [h(\mathbf{r}) - \lambda]v(E,\mathbf{r}) &= Ev(E,\mathbf{r}),\end{aligned} \tag{1}$$

where λ is the Fermi energy, h is the sum of the kinetic energy and the HF mean field potential, and Δ is the pairing potential; u and v are the upper and lower components of the quasiparticle wave function associated with the quasiparticle energy E, which we choose to be positive. In this work, we assume spherical symmetry as in the RHB approach, so that the HFB equations depend only on the radial coordinate r and they can be solved directly in r space.

We shall only consider bound systems, i.e., cases in which λ is negative. The reason is that, if λ becomes positive, there are states with $0 \leqslant E \leqslant \lambda$ whose wave functions u, v do not decrease exponentially at large distances [4]. Then, the matter density built with v^2 does not vanish asymptotically, and the nucleus is unbound. For negative λ, the spectrum consists of a discrete part for E less than $-\lambda$ and a continuous part for E above $-\lambda$. To calculate the continuum spectrum, the HFB equations should be solved with scattering type boundary conditions for the upper components of the HFB wave functions [5]. Since the continuum-HFB calculations are rather heavy, the continuum spectrum is usually discretized by imposing box boundary conditions, i.e., the condition that the HFB wave functions vanish at a given distance from the nucleus. This is sufficient for our present purpose provided that the box radius is properly chosen. We have checked that our results obtained with a box radius of 20 fm are very close to those of a full continuum calculation. Thus, most of the results presented here have been obtained by imposing box boundary conditions. Only the results discussed in Sec. III B are obtained with scattering-type boundary conditions.

In the present HFB calculations, the mean field is calculated with a Skyrme-type force, while for the pairing channel, we use a zero-range interaction with the following density dependence:

$$V(\mathbf{r}_1 - \mathbf{r}_2) = V_0\left[1 - x\left(\frac{\rho(r)}{\rho_0}\right)^{\gamma}\right]\delta(\mathbf{r}_1 - \mathbf{r}_2). \tag{2}$$

The value of ρ_0 is 0.16 fm^{-3}, corresponding approximately to the nuclear matter saturation density given by SLy4 and SkI4. We choose $x = 0.5$ to represent a pairing force half-way between a pure volume and pure surface interaction. As for γ, we simply take $\gamma = 1$, a choice compatible with the conclusions of the study made in Ref. [17] about the influence of γ on the asymptotics of nucleon distributions. The quasiparticle energy cutoff is equal to 70 MeV, and the maximum value of j is 15/2. The strength V_0 is chosen so as to reproduce the gaps extracted from the odd-even mass differences (in the regions where such experimental data are available), i.e., V_0 is adjusted to be -365 and -290 MeV fm^3(-350 and -300 MeV fm^3) for the Ca and Zr isotopes calculated with SLy4 (SkI4).

III. RESULTS OF HFB CALCULATIONS

A. Separation energies, neutron radii, and HF results

The two-neutron separation energy is defined as

$$S_{2n}(N,Z) = E(N,Z) - E(N-2,Z), \tag{3}$$

where $E(N, Z)$ is the total energy of the isotope with N neutrons and Z protons. The two-neutron separation energies for Ca and Zr isotopes are shown in Figs. 1 and 2. We display in these figures only the separation energies for the bound nuclei, i.e., those having a negative chemical potential in the HFB calculations. For instance, the separation energy is still positive in ^{64}Ca with SkI4-HFB ($S_{2n} = 0.2$ MeV) but the chemical potential is already positive and equal to 0.24 MeV. We thus define as the drip-line nucleus the last isotope having both positive separation energy and negative chemical potential. The shown results correspond to box-HFB calculations, which give practically the same S_{2n} values as continuum-HFB calculations.

The most important fact we can observe in Fig. 1 is the large difference between the drip-line location predicted by

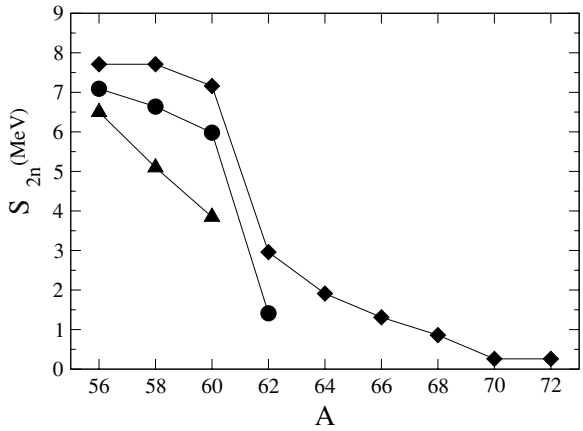

FIG. 1. Two-neutron separation energies for Ca isotopes calculated with SLy4-HFB (triangles), SkI4-HFB (circles), and RHB (diamonds). The RHB results correspond to Ref. [8].

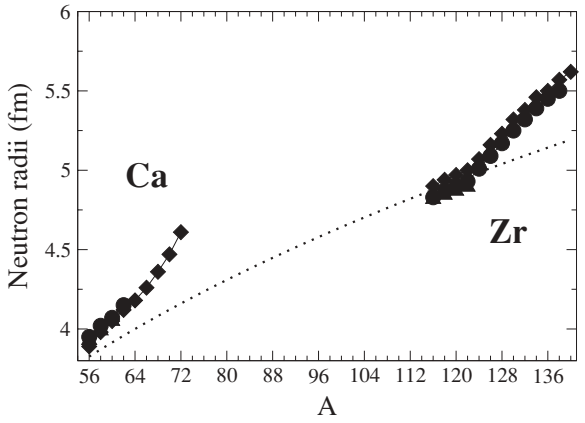

FIG. 3. Neutron radii for Ca and Zr isotopes. Symbols same as in Fig. 1; RHB results correspond to Refs. [8,9]. Radii calculated as $r_0 A^{1/3}$ ($r_0 = 1$ fm) are shown by a dotted line.

the Skyrme-HFB with SLy4 and SkI4 and that predicted by the RHB calculations of Ref. [8] for the Ca isotopes. It can be seen that for Skyrme forces, the drip line is located at ^{62}Ca (^{60}Ca) with SkI4 (SLy4), while for RHB calculations, the drip line extends up to ^{72}Ca. It must be noted that in Ref. [13], the two-neutron separation energy was found to be still positive in ^{78}Ca with the interaction SkM*. In any case, with the two Skyrme parametrizations adopted here, the region in which a giant halo could exist in Ca isotopes cannot be explored, since the last bound nucleus is reached before.

In the Zr isotopes, differences also occur among the model predictions. As seen in Fig. 2, for the force SLy4, the drip line is located at ^{122}Zr, whereas for SkI4, it is at ^{138}Zr. The latter result is similar to the RHB prediction in which the drip line is located at ^{140}Zr.

We check now whether our nonrelativistic model can predict a giant neutron halo structure by analyzing the neutron radii, which are shown in Fig. 3. As mentioned before, for Ca isotopes, the neutron drip line is reached before the halo structure starts to be formed for both the adopted Skyrme parametrizations. The same is happening for Zr isotopes if one uses the SLy4 force. However, in the case of SkI4, the situation is very different, with a change in the slope of neutron radii around $A = 122$ and values close to those of RHB.

To understand better why the drip line is so model dependent, Figs. 4 and 5 show the HF energies of the bound states close to the Fermi level in Ca and Zr isotopes, respectively. For Ca isotopes, we can see that apart from a different splitting of the $1f$ and $2p$ states, the two Skyrme forces give a rather similar pattern for the bound spectrum. The HF drip-line nucleus is ^{60}Ca with both SLy4 and SkI4; ^{62}Ca is not bound since the state $1g9/2$ remains slightly unbound with the two forces, at variance with the RMF calculations in which this state becomes weakly bound at $A = 62$ [8]. Because of this fact, the drip line in the RHB calculations is extended up to the region where the giant halo can be formed, in contrast with the HFB calculations of Ca isotopes based on SLy4 or SkI4. It must be noted, however, that this tendency is not obeyed by the Skyrme SkM* parametrization, which gives a bound $1g9/2$ orbital in the Ca isotopes with $A \geqslant 60$ resulting in a drip line located at higher A [13].

For Zr isotopes, the structure of the HF bound spectrum is not the same for the two adopted Skyrme parametrizations. We

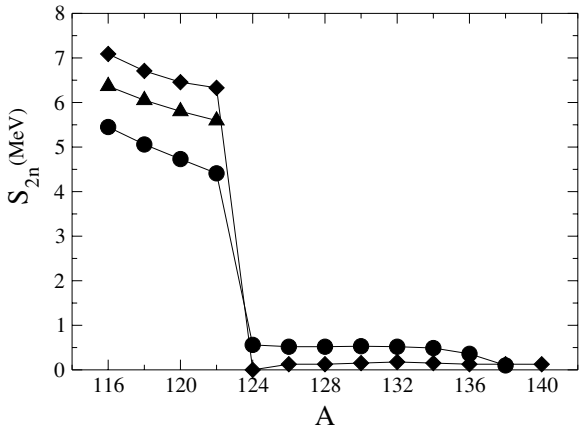

FIG. 2. Same as Fig. 1, but for Zr isotopes. RHB results correspond to Ref. [9].

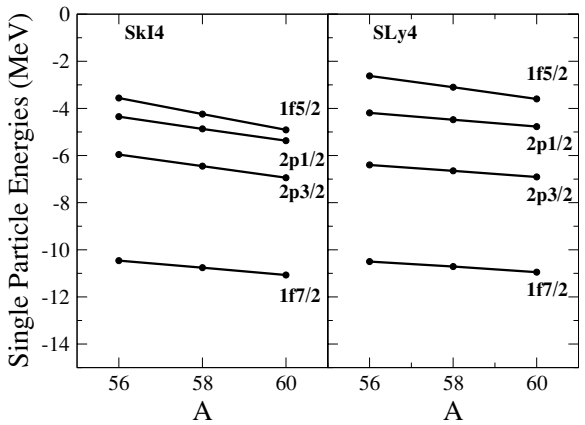

FIG. 4. SkI4-HF (left) and SLy4-HF (right) neutron single-particle energies for bound states in Ca isotopes.

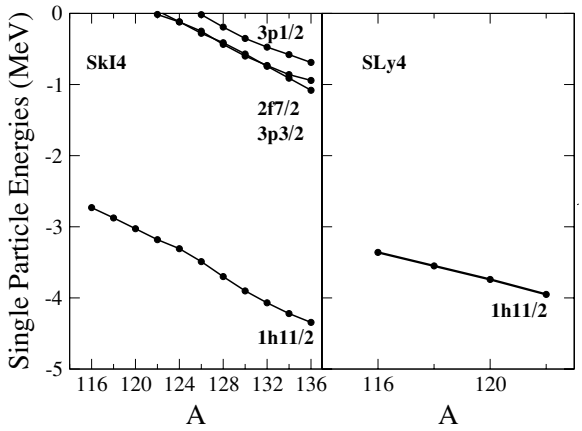

FIG. 5. Same as Fig. 4, but for Zr isotopes.

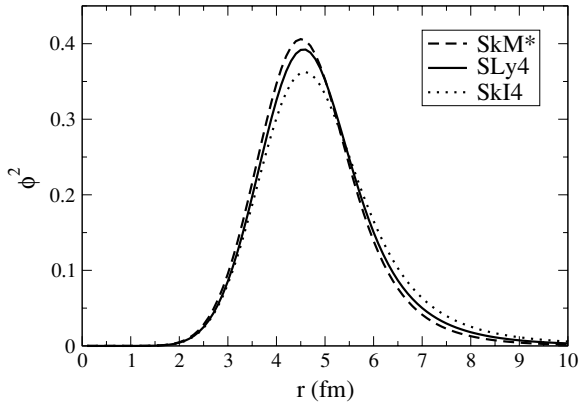

FIG. 6. Square of the $1g9/2$ wave function with the forces SkM*, SLy4, and SkI4 in ^{60}Ca.

can observe that at $A = 122$, the state $3p3/2$ becomes weakly bound with SkI4, while it remains slightly unbound with SLy4. This allows one to shift the drip line with SkI4, the states $2f7/2$ and $3p1/2$ becoming then weakly bound at $A = 124$ and 126, respectively. This is similar to what happens in the RMF calculations and explains why both the SkI4-HFB and the RHB calculations provide a halo structure in Zr isotopes. How these weakly bound HF states contribute to the halo structure in the presence of pairing correlations is discussed in the next subsection.

Let us now analyze the elements responsible for the differences found in the single-particle spectra and in the drip-line predictions. We can write the HF equation as

$$\frac{\hbar^2}{2m}\left[-\frac{d^2}{dr^2}\psi(r)+\frac{l(l+1)}{r^2}\psi(r)\right]+V_{\rm eq}(r,\epsilon)\psi(r)=\epsilon\psi(r), \tag{4}$$

where the equivalent potential $V_{\rm eq}$ reads

$$V_{\rm eq}(r,\epsilon)=\frac{m^*(r)}{m}U_0(r)+\frac{m^*(r)}{m}U_{{\rm so},lj}(r) - \frac{m^{*2}(r)}{2m\hbar^2}\left(\frac{\hbar^2}{2m^*(r)}\right)^{\prime 2}+\frac{m^*(r)}{2m}\left(\frac{\hbar^2}{2m^*(r)}\right)^{\prime\prime} + \left[1-\frac{m^*(r)}{m}\right]\epsilon. \tag{5}$$

with $U_{{\rm so},lj}(r) = U_{\rm so}(r)\times[j(j+1)-l(l+1)-3/4]$. The local equivalent potential $V_{\rm eq}$ takes into account the effects of the Skyrme-HF effective mass, and the exact HF wave function $\phi(lj)$ of energy ϵ is related (up to a normalization factor) to the solution ψ of Eq. (4) by the relation $\psi = (m^*/m)^{1/2}\phi$. The functions $U_0(r)$ and $U_{\rm so}(r)$ are the central and spin-orbit HF potentials, whereas $m^*(r)$ is the effective mass [18]. The first two terms of Eq. (5) are the main contributions, the next two terms are small corrections, and the last term has a small contribution for states in the vicinity of zero energy.

We first consider the Ca isotopes, as illustrated by the nucleus ^{60}Ca and the single-particle state $1g9/2$. For this nucleus, the state $1g9/2$ is bound with the force SkM* ($\epsilon \sim -1.3$ MeV) [13], whereas it is a single-particle resonance with SLy4 ($\epsilon \sim 0.3$ MeV) and with SkI4 ($\epsilon \sim 1$ MeV). We display in Fig. 6 the square of the HF $1g9/2$ wave functions in ^{60}Ca calculated with SkM*, SLy4, and SkI4. Their general behaviors are quite similar up to more than twice the nuclear radius.

The four functions (a) the mean field $U_0(r)$, (b) the mean field multiplied by the effective mass, $U_{0m^*}(r) = U_0(r)[m^*(r)/m]$, (c) the spin-orbit term $U_{{\rm so},lj}(r)$, and (d) the spin-orbit term multiplied by the effective mass, $U_{{\rm so},lj^*}(r)$, are calculated with the three parametrizations and displayed in Fig. 7. They are shown in the radial region around 4.5 fm where the square of the single-particle wave function $1g9/2$ has its maximum. In this region, one sees that the potentials $U_{0m^*}(r)$ and $U_{{\rm so},lj^*}(r)$ of SkM* are deeper than those of SkI4 and SLy4. One can observe that the effective mass $m^*(r)$ plays an important role in shifting down the $1g9/2$ single-particle energy of SkM* to below the values of SkI4 and SLy4. In the nucleus ^{60}Ca, the values of the neutron effective mass m_n^*/m at $r = 0$ are 0.788, 0.680, and 0.606 for SkM*, SLy4, and SkI4, respectively; whereas at $r = 4.6$ fm, they are 0.946, 0.842, and 0.814. This explains why U_{0m^*} is deepest for SkM*, although U_0(SkM*) itself is the least attractive.

We perform a similar analysis for Zr isotopes. We consider the case of ^{122}Zr and the HF wave function of the state $3p3/2$ calculated with the two parametrizations SLy4 and SkI4. This state is bound in the HF spectrum with SkI4 ($\epsilon \sim -0.02$ MeV),

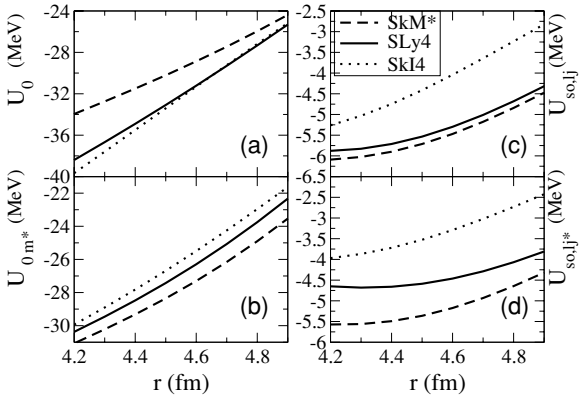

FIG. 7. Four functions defined in text calculated with the three parametrizations in ^{60}Ca for $l = 4$ and $j = 9/2$.

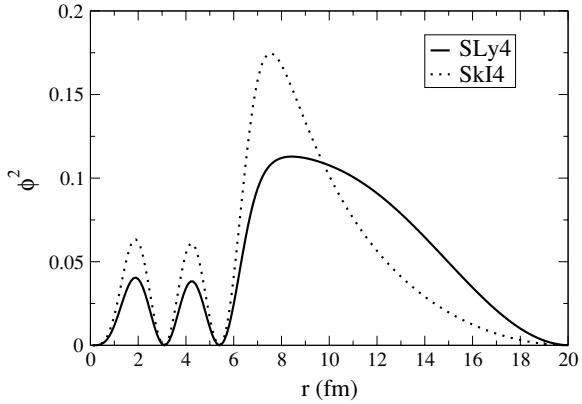

FIG. 8. Square of the $3p3/2$ wave function with forces SLy4 and SkI4 in ^{122}Zr.

but it is unbound with SLy4 ($\epsilon \sim 0.6$ MeV). We show in Fig. 8 the square of the wave function $3p3/2$ calculated with the two forces.

Figure 9 shows the four functions $U_0(r)$, $U_{0m^*}(r)$, $U_{\mathrm{so},lj}(r)$, and $U_{\mathrm{so},lj^*}(r)$ calculated with SLy4 and SkI4. They are plotted in the radial region around 8 fm where the square of the single-particle wave function has its highest maximum. The differences between the top and bottom panels are negligible, reflecting the fact that around $r = 8$ fm, the effective mass m_n^*/m in ^{122}Zr is 0.994 and 0.990 for SLy4 and SkI4, respectively. Furthermore, one can see that the mean field potential is sizably deeper with SkI4, while the differences in the spin-orbit potentials are much less important.

From this study, we can see the decisive role of the effective mass upon the energy of single-particle states when their wave functions are around the surface region. In the example of the $1g9/2$ state in ^{60}Ca, the relative positions of the central and spin-orbit potentials are much affected by the m^*/m factor. When the states are outside the surface region and the m^*/m factor becomes close to unity, the single-particle energies are directly governed by the mean field $U_0(r)$, which in turn depends on neutron-proton symmetry properties such as the symmetry energy coefficient.

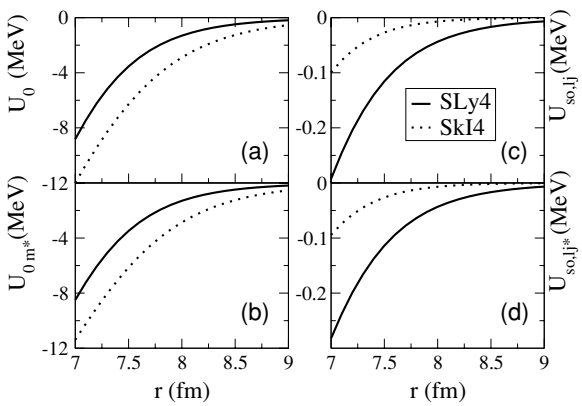

FIG. 9. Four functions calculated with the forces SLy4 and SkI4 in ^{122}Zr for $l = 1$ and $j = 3/2$.

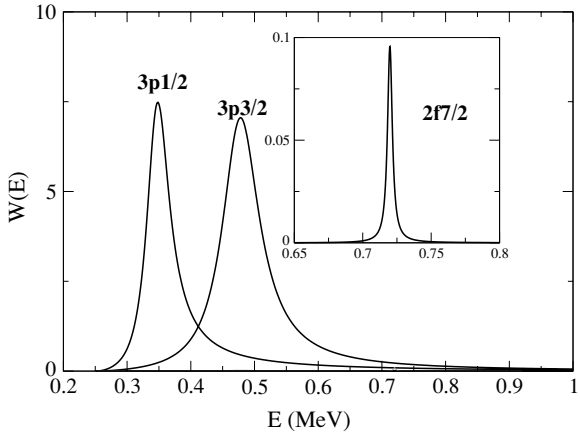

FIG. 10. Occupation profiles $W(E)$ (in MeV^{-1}) for three states in ^{132}Zr, calculated with SkI4-HFB.

B. Structure of the giant halo in Zr isotopes

In the presence of pairing correlations, the bound single-particle states shown in Fig. 5 are becoming quasiparticle resonances. To describe them properly, we solved the HFB equations with scattering-type boundary conditions. To reduce the numerical effort, we employed scattering boundary conditions only for the quasiparticle states with the energy $-\lambda < E < 15$ MeV because they are the most affected by pairing correlations, while for the other states we used box boundary conditions.

With the continuum HFB solutions, we can calculate how the occupation probability changes in the region around a resonance. This information is provided by the quantity

$$W(E) = \int_0^R dr r^2 v_E^2(r), \tag{6}$$

where v is the lower component of the HFB wave function, and R is taken equal to 20 fm. As an example, we show in Fig. 10 the values of $W(E)$ corresponding to the states $3p1/2$, $3p3/2$, and $2f7/2$ in the nucleus ^{132}Zr. In this nucleus, the quasiparticle continuum starts at the energy $E = -\lambda = 0.251$ MeV.

By integrating the function $W(E)$ over an energy interval in which it has a significant value, we can associate to each resonance an occupation probability n, i.e.,

$$n = \int_{E_1}^{E_2} W(E) dE. \tag{7}$$

The occupation probabilities of the relevant resonant states in Zr isotopes are shown in Fig. 11. It can be seen that the occupation probabilities corresponding to the weakly bound states increase progressively when going from ^{124}Zr to ^{138}Zr. Thus, these states contribute significantly to the pairing correlations.

To analyze the structure of the halo, we plot in Fig. 12 the quantity

$$R_{lj}(r) = \frac{\rho_{lj}(r)}{\rho(r)}, \tag{8}$$

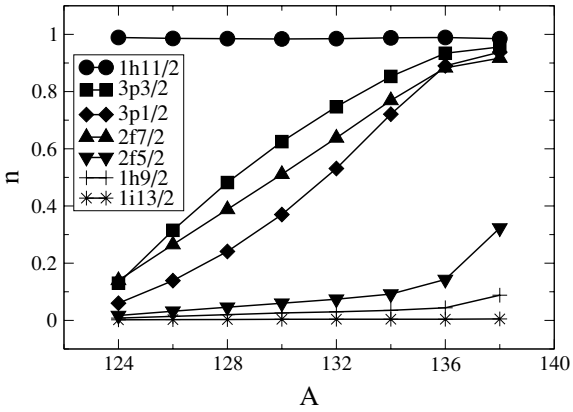

FIG. 11. Occupation probabilities for Zr isotopes, calculated with SkI4-HFB.

where ρ and ρ_{lj} are the total neutron density and the density corresponding to the channel (l, j), respectively. From Fig. 12, we can clearly see that at large distances, the dominant contribution to the neutron density is given by the p states, which are less confined by the centrifugal barrier than are the other states with higher (l, j) values. This structure of the giant halo obtained by using the SkI4-HFB model is very similar to that given by the relativistic calculations [9,11].

By comparing the neutron densities of ^{124,138}Zr with that of the reference nucleus ^{122}Zr we can estimate the number of neutrons involved in the outer skin and halo regions. We thus find that this number is 1.15 neutrons (14.27 neutrons) in the region beyond 6.8 fm (5.4 fm) in ^{124}Zr (^{138}Zr). Alternatively, one can evaluate the number of neutrons in the weakly bound orbitals and the resonant continuum as suggested in Ref. [13], which gives 1.97 and 15.92 neutrons in ^{124}Zr and ^{138}Zr, respectively.

C. Antihalo effect

We turn now to the analysis of the so-called antihalo effect, which was mainly discussed in light nuclei close to the neutron drip line [16]. This effect is associated with a reduction of the neutron radii by the pairing correlations.

In Zr isotopes, the pairing correlations affect the neutron halo through the p and f states. We take as an illustration the case of ^{124}Zr for which the neutron radius is equal to 5.08 (5.01) fm in HF (HFB). We adopt a spherical symmetry scheme for the present discussion since it is found in RMF calculations that Zr isotopes are predicted to be spherical beyond $A = 122$ [9]. In ^{124}Zr, the $3p3/2$ state is half occupied, while $2f7/2$ (weakly bound) is empty in HF. When pairing correlations are switched on within HFB, the occupancy of the $3p3/2$ state is much reduced and that of the $2f7/2$ is enhanced, as one can observe in Fig. 11.

Bennaceur *et al.* [16] analyzed the antihalo effect in terms of the asymptotic behavior of the neutron densities calculated in HF and in HFB. In the latter case, the existence of a finite pairing gap due to pairing correlations gave a faster decaying tail in the neutron density. The states responsible for this effect were those close to the Fermi energy, i.e., those with single-particle energies $\epsilon \sim \lambda$. We plot in Fig. 13 the neutron wave function tails of the states $3p3/2$ (top) and $2f7/2$ (bottom) calculated in HF and HFB for ^{124}Zr. To compare the HF and HFB wave functions, we plotted in the HFB case the lower component of the quasiparticle wave functions, normalized to unity. In the two insets of the figure, we display the tails of the wave functions in logarithmic scale. One can observe that at large distances, the HFB wave functions decay faster than the corresponding HF ones in both cases. This confirms the argument given by Bennaceur *et al.* [16] and explains in part why the HFB neutron radius is smaller than the HF one. However, it should be noted that the antihalo effect is not only due to the slope of the wave functions at large distances. Another contribution to this effect is related to the occupancies of the states in HF and HFB. As mentioned before, when pairing correlations are taken into account, the occupancy of the $3p3/2$ state is reduced while that of $2f7/2$ is enhanced. Since $2f7/2$ has a smaller radial extension than $3p3/2$ due to the centrifugal barrier, the HFB radius is less than the HF one. We can thus say that a stronger effect of the pairing correlations

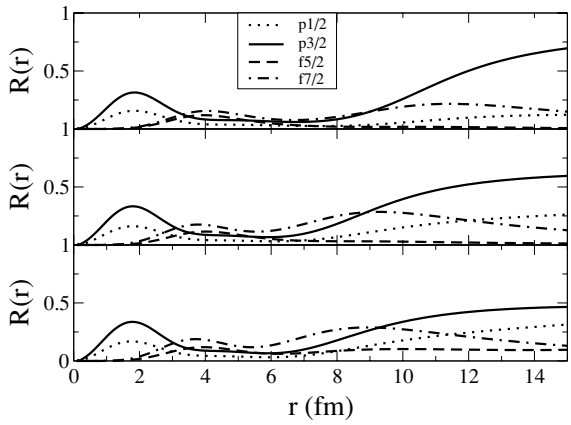

FIG. 12. Contributions of different (l, j) channels to the total neutron density for ^{124}Zr (top), ^{132}Zr (middle), and ^{138}Zr (bottom). The interaction is SkI4.

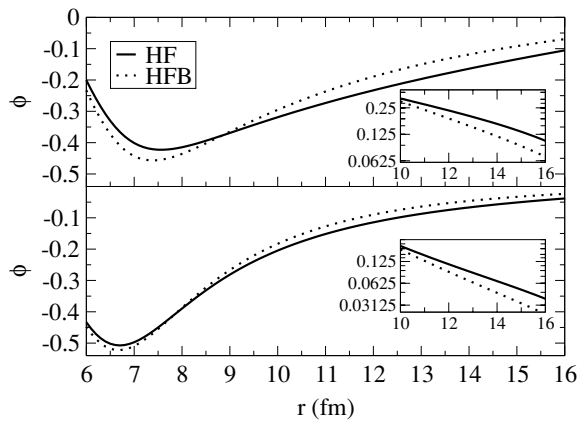

FIG. 13. HF (full lines) and HFB (dotted lines) neutron wave functions for the states $3p3/2$ (top) and $2f7/2$ (bottom) in ^{124}Zr. Insets show the tails of the wave functions plotted in logarithmic scale. The interaction is SkI4.

upon the reduction of the neutron radius is expected when close to the Fermi level one finds a weakly bound low-l state ($3p3/2$ in our case) together with states with higher angular momenta ($2f7/2$ in our case).

We conclude, however, by stressing that the antihalo effect caused by pairing is not strong enough to prevent the formation of a neutron giant halo close to the drip line for Zr isotopes, as we have shown in the previous sections.

IV. CONCLUSIONS

In this work, we have examined the evolution of the nuclear structure of Zr isotopes at large neutron excess, giving special attention to the far out region of neutron densities. This is motivated by the predictions of the RHB approach which indicate the presence of a giant neutron halo in these nuclei. We have used a different approach, namely, the Skyrme-HFB model. We find that in this isotopic chain, the presence or absence of giant halos depends essentially on the location of the predicted neutron drip line. Thus, there is a strong model dependence in this type of study, as illustrated by the results obtained with the Skyrme forces SLy4 and SkI4.

For the drip line to be displaced toward heavier isotopes, a necessary condition is that some HF orbitals become bound when A increases. In this case, additional bound neutrons can be accommodated, and bound nuclei of heavier mass can be formed. An illustration of this situation is provided by the Zr isotopes, for which this necessary condition is fulfilled by some model like SkI4 but not by SLy4. Once the necessary condition is realized, a neutron halo may exist if some of the weakly bound HF orbitals correspond to low angular momenta ($3p3/2$ and $3p1/2$ in the case of Zr) so that the centrifugal barrier is weak enough to let the wave functions extend far out.

Thus, the decisive factor is the HF mean field which governs the HF single-particle spectrum, while the pairing correlations play a lesser role. For states that are relatively outside the nuclear surface, the single-particle energies depend mostly on the HF mean field, i.e., on the neutron-proton symmetry properties of the energy functional. On the other hand, the states located near the nuclear surface have their single-particle energies influenced by the value of the effective mass in that region. Actually, experimental determination of neutron drip lines in some nuclei would help place bounds on the values of effective masses.

We have also seen that the pairing correlations can lead to the antihalo effect. This can be understood by analyzing the occupation probabilities and the wave function tails of the least bound (lj) orbitals. Finally, we note that this antihalo effect is not strong enough to prevent the formation of a neutron giant halo structure in neutron-rich Zr isotopes.

[1] Proceedings of the 17th International Conference on Cyclotrons and Their Applications, October 2004, Tokyo.

[2] M. Bender, P.-H. Heenen, and P.-G. Reinhard, Rev. Mod. Phys. **75**, 121 (2003).

[3] J. Meng, H. Toki, S. G. Zhou, S. Q. Zhang, W. H. Long, and L. S. Geng, Prog. Part. Nucl. Phys. **57**, 470 (2006).

[4] J. Dobaczewski, H. Flocard, and J. Treiner, Nucl. Phys. **A422**, 103 (1984); J. Dobaczewski, W. Nazarewicz, T. R. Werner, J.-F. Berger, C. R. Chinn, and J. Dechargé, Phys. Rev. C **53**, 2809 (1996).

[5] M. Grasso, N. Sandulescu, Nguyen Van Giai, and R. J. Liotta, Phys. Rev. C **64**, 064321 (2001).

[6] J. Meng and P. Ring, Phys. Rev. Lett. **77**, 3963 (1996); J. Meng, Nucl. Phys. **A635**, 3 (1998).

[7] B. V. Carlson and D. Hirata, Phys. Rev. C **62**, 054310 (2000).

[8] J. Meng, H. Toki, J. Y. Zeng, S. Q. Zhang, and S.-G. Zhou, Phys. Rev. C **65**, 041302 (2002).

[9] J. Meng and P. Ring, Phys. Rev. Lett. **80**, 460 (1998).

[10] S. Q. Zhang, J. Meng, H. Toki, I. Tanihata, and S.-G. Zhou, Science China Ser. G **46**, 632 (2003).

[11] N. Sandulescu, L. S. Geng, H. Toki, and G. C. Hillhouse, Phys. Rev. C **68**, 054323 (2003).

[12] S. Mizutori, J. Dobaczewski, G. A. Lalazissis, W. Nazarewicz, and P.-G. Reinhard, Phys. Rev. C **61**, 044326 (2000).

[13] J. Terasaki, S. Q. Zhang, S. G. Zhou, and J. Meng, Phys. Rev. C **74**, 054318 (2006).

[14] J. Meng, Phys. Rev. C **57**, 1229 (1998); M. Del Estal, M. Centelles, X. Viñas, and S. K. Patra, Phys. Rev. C **63**, 044321 (2001).

[15] P.-G. Reinhard and H. Flocard, Nucl. Phys. **A584**, 467 (1995).

[16] S. A. Fayans, S. V. Tolokonnikov, and D. Zawischa, Phys. Lett. **B491**, 245 (2000); K. Bennaceur, J. Dobaczewski, and M. Ploszajczak, *ibid.* **B496**, 154 (2000).

[17] J. Dobaczewski, W. Nazarewicz, and P.-G. Reinhard, Nucl. Phys. **A693**, 361 (2001).

[18] E. Chabanat, P. Bonche, P. Haensel, J. Meyer, and R. Schaeffer, Nucl. Phys. **A635**, 231 (1998); **A643**, 441(E) (1998).